Monolithic erbium- and ytterbium-doped microring lasers on silicon chips

Jonathan D. B. Bradley,[1] Ehsan Shah Hosseini,[1] Purnawirman,[1] Zhan Su,[1] Thomas N. Adam,[2] Gerald Leake,[2] Douglas Coolbaugh,[2] and Michael R. Watts[1,*]

[1]*Photonic Microsystems Group, Research Laboratory of Electronics, Massachusetts Institute of Technology, 77 Massachusetts Avenue, Cambridge, Massachusetts 02139, USA*

[2]*College of Nanoscale Science and Engineering, University at Albany, State University of New York, 257 Fuller Road, Albany, New York 12203, USA*

[*]*mwatts@mit.edu*

Abstract: We demonstrate monolithic 160-µm-diameter rare-earth-doped microring lasers using silicon-compatible methods. Pump light injection and laser output coupling are achieved via an integrated silicon nitride waveguide. We measure internal quality factors of up to 3.8×10^5 at 980 nm and 5.7×10^5 at 1550 nm in undoped microrings. In erbium- and ytterbium-doped microrings we observe single-mode 1.5-µm and 1.0-µm laser emission with slope efficiencies of 0.3 and 8.4%, respectively. Their small footprints, tens of microwatts output powers and sub-milliwatt thresholds introduce such rare-earth-doped microlasers as scalable light sources for silicon-based microphotonic devices and systems.

©2014 Optical Society of America

OCIS codes: (130.0130) Integrated optics; (140.0140) Lasers and laser optics; (140.3500) Lasers, erbium; (140.3615) Lasers, ytterbium; (140.3948) Microcavity devices.

References and links

1. G. T. Reed, "Device physics: the optical age of silicon," Nature **427**(6975), 595–596 (2004).
2. M. Lipson, "Guiding, modulating, and emitting light on silicon—challenges and opportunities," J. Lightwave Technol. **23**(12), 4222–4238 (2005).
3. B. Jalali and S. Fathpour, "Silicon photonics," J. Lightwave Technol. **24**(12), 4600–4615 (2006).
4. A. H. J. Yang, S. D. Moore, B. S. Schmidt, M. Klug, M. Lipson, and D. Erickson, "Optical manipulation of nanoparticles and biomolecules in sub-wavelength slot waveguides," Nature **457**(7225), 71–75 (2009).
5. J. Sun, E. Timurdogan, A. Yaacobi, E. S. Hosseini, and M. R. Watts, "Large-scale nanophotonic phased array," Nature **493**(7431), 195–199 (2013).
6. L. Pavesi, "Routes towards silicon-based lasers," Mater. Today **8**(1), 18–25 (2005).
7. D. Liang and J. E. Bowers, "Recent progress in lasers on silicon," Nat. Photonics **4**(8), 511–517 (2010).
8. Z. Fang, Q. Y. Chen, and C. Z. Zhao, "A review of recent progress in lasers on silicon," Opt. Laser Technol. **46**, 103–110 (2013).
9. Y. Hibino, T. Kitagawa, M. Shimizu, F. Hanawa, and A. Sugita, "Neodymium-doped silica optical waveguide laser on silicon substrate," IEEE Photon. Technol. Lett. **1**(11), 349–350 (1989).
10. T. Kitagawa, M. Hattori, M. Shimizu, Y. Ohmori, and M. Kobayashi, "Guided-wave laser based on erbium-doped silica planar lightwave circuit," IEEE Photon. Technol. Lett. **27**, 334–335 (1991).
11. K. Hattori, F. Bilodeau, B. Malo, J. Albert, D. C. Jihnson, T. Kitagawa, Y. Hibino, S. Thériault, and K. O. Hill, "Single-frequency Er^{3+}-doped silica-based planar waveguide laser with integrated photo-imprinted Bragg reflectors," Electron. Lett. **30**(16), 1311–1312 (1994).
12. J. Hübner, S. Guldberg-Kjaer, M. Dyngaard, Y. Shen, C. L. Thomsen, S. Balslev, C. Jensen, D. Zauner, and T. Feuchter, "Planar Er- and Yb-doped amplifiers and lasers," Appl. Phys. B **73**(5-6), 435–438 (2001).
13. B. Unal, M. C. Netti, M. A. Hassan, P. J. Ayliffe, M. D. B. Charlton, F. Lahoz, N. M. B. Perney, D. P. Shepherd, C.-Y. Tai, J. S. Wilkinson, and G. J. Parker, "Neodymium-doped tantalum pentoxide waveguide lasers," IEEE J. Quantum Electron. **41**(12), 1565–1573 (2005).
14. D. Pudo, H. Byun, J. Chen, J. Sickler, F. X. Kärtner, and E. P. Ippen, "Scaling of passively mode-locked soliton erbium waveguide lasers based on slow saturable absorbers," Opt. Express **16**(23), 19221–19231 (2008).
15. A. Z. Subramani, C. J. Oton, D. P. Shepherd, and J. S. Wilkinson, "Erbium-doped waveguide laser in tantalum pentoxide," IEEE Photon. Technol. Lett. **22**(21), 1571–1573 (2010).
16. J. D. B. Bradley, R. Stoffer, L. Agazzi, F. Ay, K. Wörhoff, and M. Pollnau, "Integrated Al_2O_3:Er^{3+} ring lasers on silicon with wide wavelength selectivity," Opt. Lett. **35**(1), 73–75 (2010).
17. E. H. Bernhardi, H. A. G. M. van Wolferen, L. Agazzi, M. R. H. Khan, C. G. H. Roeloffzen, K. Wörhoff, M. Pollnau, and R. M. de Ridder, "Ultra-narrow-linewidth, single-frequency distributed feedback waveguide laser in Al_2O_3:Er^{3+} on silicon," Opt. Lett. **35**(14), 2394–2396 (2010).

#206846 - $15.00 USD Received 20 Feb 2014; revised 29 Apr 2014; accepted 29 Apr 2014; published 13 May 2014

18. E. H. Bernhardi, H. A. G. M. van Wolferen, K. Wörhoff, R. M. de Ridder, and M. Pollnau, "Highly efficient, low-threshold monolithic distributed-Bragg-reflector channel waveguide laser in $Al_2O_3:Yb^{3+}$," Opt. Lett. **36**(5), 603–605 (2011).
19. J. Purnawirman, J. Sun, T. N. Adam, G. Leake, D. Coolbaugh, J. D. Bradley, E. Shah Hosseini, and M. R. Watts, "C- and L-band erbium-doped waveguide lasers with wafer-scale silicon nitride cavities," Opt. Lett. **38**(11), 1760–1762 (2013).
20. M. Belt, T. Huffman, M. L. Davenport, W. Li, J. S. Barton, and D. J. Blumenthal, "Arrayed narrow linewidth erbium-doped waveguide-distributed feedback lasers on an ultra-low-loss silicon-nitride platform," Opt. Lett. **38**(22), 4825–4828 (2013).
21. E. Shah Hosseini, Purnawirman, J. D. B. Bradley, J. Sun, G. Leake, T. N. Adam, D. Coolbaugh, and M. R. Watts, "CMOS compatible 75 mW erbium doped distributed feedback laser," Opt. Lett. (submitted).
22. D. K. Armani, T. J. Kippenberg, S. M. Spillane, and K. J. Vahala, "Ultra-high-*Q* toroid microcavity on a chip," Nature **421**(6926), 925–928 (2003).
23. M. Borselli, T. J. Johnson, and O. Painter, "Beyond the Rayleigh scattering limit in high-*Q* silicon microdisks: theory and experiment," Opt. Express **13**(5), 1515–1530 (2005).
24. A. Polman, B. Min, J. Kalkman, T. J. Kippenberg, and K. J. Vahala, "Ultralow-threshold erbium-implanted toroidal microlaser on silicon," Appl. Phys. Lett. **84**(7), 1037–1039 (2004).
25. L. Yang, T. Carmon, B. Min, S. M. Spillane, and K. J. Vahala, "Erbium-doped and Raman microlasers on a silicon chip fabricated by the sol-gel process," Appl. Phys. Lett. **86**(9), 091114 (2005).
26. M. Borselli, *High-Q Microresonators as Lasing Elements for Silicon Photonics* (Ph.D. Thesis, California Institute of Technology, 2006).
27. T. J. Kippenberg, J. Kalkman, A. Polman, and K. J. Vahala, "Demonstration of an erbium-doped microdisk laser on a silicon chip," Phys. Rev. A **74**(5), 051802 (2006).
28. E. P. Ostby, L. Yang, and K. J. Vahala, "Ultralow-threshold $Yb^{3+}:SiO_2$ glass laser fabricated by the solgel process," Opt. Lett. **32**(18), 2650–2652 (2007).
29. H.-S. Hsu, C. Cai, and A. M. Armani, "Ultra-low-threshold Er:Yb sol-gel microlaser on silicon," Opt. Express **17**(25), 23265–23271 (2009).
30. S. Mehrabani and A. M. Armani, "Blue upconversion laser based on thulium-doped silica microcavity," Opt. Lett. **38**(21), 4346–4349 (2013).
31. A. J. Maker and A. M. Armani, "Nanowatt threshold, alumina sensitized neodymium laser integrated on silicon," Opt. Express **21**(22), 27238–27245 (2013).
32. D. S. Gardner and M. L. Brongersma, "Microring and microdisk optical resonators using silicon nanocrystals and erbium prepared using silicon technology," Opt. Mater. **27**(5), 804–811 (2005).
33. J. S. Chang, S. C. Eom, G. Y. Sung, and J. H. Shin, "On-chip, planar integration of Er doped silicon-rich silicon nitride microdisk with SU-8 waveguide with sub-micron gap control," Opt. Express **17**(25), 22918–22924 (2009).
34. D. W. Prather, B. Redding, T. Creazzo, E. Marchena, and S. Shi, "Integration of silicon nanocrystals and erbium ring cavities for a silicon pumped $Er:SiO_2$ laser," J. Nanosci. Nanotechnol. **10**(3), 1643–1649 (2010).
35. M. Ghulinyan, R. Guider, G. Pucker, and L. Pavesi, "Monolithic whispering-gallery mode resonators with vertically coupled integrated bus waveguides," IEEE Photon. Technol. Lett. **23**(16), 1166–1168 (2011).
36. F. F. Lupi, D. Navarro-Urrios, J. Rubio-Garcia, J. Monserrat, C. Dominquez, P. Pellegrino, and B. Garrido, "Visible light emitting Si-rich Si_3N_4 μ-disk resonators for sensoristic applications," J. Lightwave Technol. **30**(1), 169–174 (2012).
37. Purnawirman, E. Shah Hosseini, A. Baldycheva, J. Sun, J. D. B. Bradley, T. N. Adam, G. Leake, D. Coolbaugh, and M. R. Watts, "Erbium-doped laser with multi-segmented silicon nitride structure," in *Optical Fiber Communication Conference Proceedings*, in Optical Fiber Communication Conference, OSA Technical Digest (online) (Optical Society of America, 2014), paper W4E.5.
38. K. Wörhoff, J. D. B. Bradley, F. Ay, D. Geskus, T. Blauwendraat, and M. Pollnau, "Reliable low-cost fabrication of low-loss $Al_2O_3:Er^{3+}$ waveguides with 5.4-dB optical gain," IEEE J. Quantum Electron. **45**(5), 454–461 (2009).
39. E. H. Bernhardi, *Bragg-Grating-Based Rare-Earth-Ion-Doped Channel Waveguide Lasers and their Applications* (Ph.D. Thesis. University of Twente, 2012).
40. J. D. B. Bradley, L. Agazzi, D. Geskus, F. Ay, K. Wörhoff, and M. Pollnau, "Gain bandwidth of 80 nm and 2 dB/cm peak gain in $Al_2O_3:Er^{3+}$ optical amplifiers on silicon," J. Opt. Soc. Am. B **27**(2), 187–196 (2010).
41. E. S. Hosseini, S. Yegnanarayanan, A. H. Atabaki, M. Soltani, and A. Adibi, "High quality planar silicon nitride microdisk resonators for integrated photonics in the visible wavelength range," Opt. Express **17**(17), 14543–14551 (2009).
42. L. Yang and K. J. Vahala, "Gain functionalization of silica microresonators," Opt. Lett. **28**(8), 592–594 (2003).
43. L. He, S. K. Özdemir, J. Zhu, and L. Yang, "Self-pulsation in fiber-coupled, on-chip microcavity lasers," Opt. Lett. **35**(2), 256–258 (2010).
44. L. He, S. K. Özdemir, and L. Yang, "Whispering gallery microcavity lasers," Laser Photon. Rev. **7**(1), 60–82 (2013).
45. G. N. van den Hoven, R. J. I. M. Koper, A. Polman, C. van Dam, J. W. M. van Uffelen, and M. K. Smit, "Net optical gain at 1.53 µm in Er-doped Al_2O_3 waveguides on silicon," Appl. Phys. Lett. **68**(14), 1886–1888 (1996).
46. E. P. Ostby and K. J. Vahala, "Yb-doped glass microcavity laser operation in water," Opt. Lett. **34**(8), 1153–1155 (2009).

#206846 - $15.00 USD Received 20 Feb 2014; revised 29 Apr 2014; accepted 29 Apr 2014; published 13 May 2014
(C) 2014 OSA

47. L. He, S. K. Özdemir, J. Zhu, W. Kim, and L. Yang, "Detecting single viruses and nanoparticles using whispering gallery microlasers," Nat. Nanotechnol. **6**(7), 428–432 (2011).

1. Introduction

Over the last several years, advances in the field of silicon photonics have lead to highly-compact, low-cost, and high-performance photonic chips for applications ranging from high-speed optical communications to lab-on-a-chip devices [1–5]. However, because of silicon's indirect bandgap and low quantum efficiency, one of the main challenges has been the development of silicon-based lasers [6–8]. Ideally such lasers should offer high performance in addition to being compact, monolithic and fabricated using standard silicon techniques to be considered as scalable light sources for silicon microphotonic systems.

Rare-earth-doped waveguide lasers (REDWLs) have shown significant promise as silicon-based lasers because they combine efficient, continuous-wave or short pulse lasing over a wide wavelength range with inexpensive, straightforward and monolithic integration methods [9–21]. In particular, rare-earth-doped aluminum oxide (Al_2O_3:RE^{3+}) has emerged as a highly versatile and robust laser medium, having recently been applied in wavelength-selective racetrack, ultra-narrow-linewidth distributed feedback (DFB) and highly-efficient distributed Bragg reflector (DBR) monolithic lasers [16–18]. Furthermore, integration of Al_2O_3:RE^{3+} DBR and DFB lasers using wafer-scale and silicon-compatible silicon nitride photonic cavity structures has been demonstrated, with up to 75 mW continuous-wave output power [19–21]. Nevertheless, integration of REDWLs into microphotonic platforms is limited by their large size and significant power consumption, with centimeter-scale cavity lengths and thresholds ranging from several to tens of milliwatts.

In an approach which drastically reduces the device size and lasing threshold, high quality factor whispering gallery mode cavities [22,23] have been doped with rare earth ions to realize visible and infrared microtoroid and microdisk lasers on silicon [24–31]. However, such lasers are isolated on the chip surface and require an external fiber to couple pump and laser light to and from the cavity, respectively. Whereas efforts have been made towards a monolithic micrometer-scale integration scheme [32–36], that is, where both microcavity and waveguide are co-integrated on the same chip, to our knowledge, no laser action has previously been demonstrated.

Here, using a design which combines Al_2O_3:RE^{3+} with silicon-compatible silicon nitride waveguides, we report on compact, low-threshold microring lasers monolithically integrated on silicon chips. The erbium- and ytterbium-doped microlasers are fully integrated with their excitation and emission bus waveguides via a flexible and high-Q cavity design and effective fabrication technique. We show sub-milliwatt threshold, single-mode lasing both at optical communications wavelengths around 1.5 μm and at 1.0 μm where biophotonic applications are of interest. Our approach allows for straightforward, dense integration of such laser sources within existing silicon-based microphotonic systems.

2. Microring laser design and fabrication

As shown in Fig. 1, our microring laser design is based on a silicon-compatible process flow which uses two silicon nitride (SiN_x) layers. The microlaser structure consists of an Al_2O_3:RE^{3+}-filled trench above five concentric silicon nitride rings, which forms the active microcavity, beside a SiN_x bus waveguide for pump injection and laser output coupling. SiN_x has a higher refractive index than Al_2O_3:RE^{3+} (n = 2 vs. n = 1.65), enabling more compact, high-refractive-index-contrast and low-loss passive photonic devices. However, to achieve net gain in the cavity and lasing, a sufficient proportion of light must propagate in the active medium (Al_2O_3:RE^{3+}). Thus, we developed a composite resonator structure which supports modes with high optical intensity overlap with the Al_2O_3:RE^{3+} layer, but also permits reduced microring diameter due to the SiN_x features. The trench also serves to confine the light and reduce the microring bending radius and enables silicon compatibility (the non-standard gain material can be deposited into the trenches outside of the silicon foundry). The segmented silicon nitride cavity design yields a highly wavelength-insensitive mode shape, allowing for

#206846 - $15.00 USD Received 20 Feb 2014; revised 29 Apr 2014; accepted 29 Apr 2014; published 13 May 2014
(C) 2014 OSA

high overlap between 980-nm pump modes and 1050-nm Yb- or 1550-nm Er-doped microring laser modes [37]. Meanwhile, the integrated double-layer silicon nitride bus waveguide allows for a high degree of control of waveguide mode properties (*i.e.* for phase-matching to the microcavity pump modes and effective coupling of pump light to the ring) and low-loss guiding of pump and laser light on the chip.

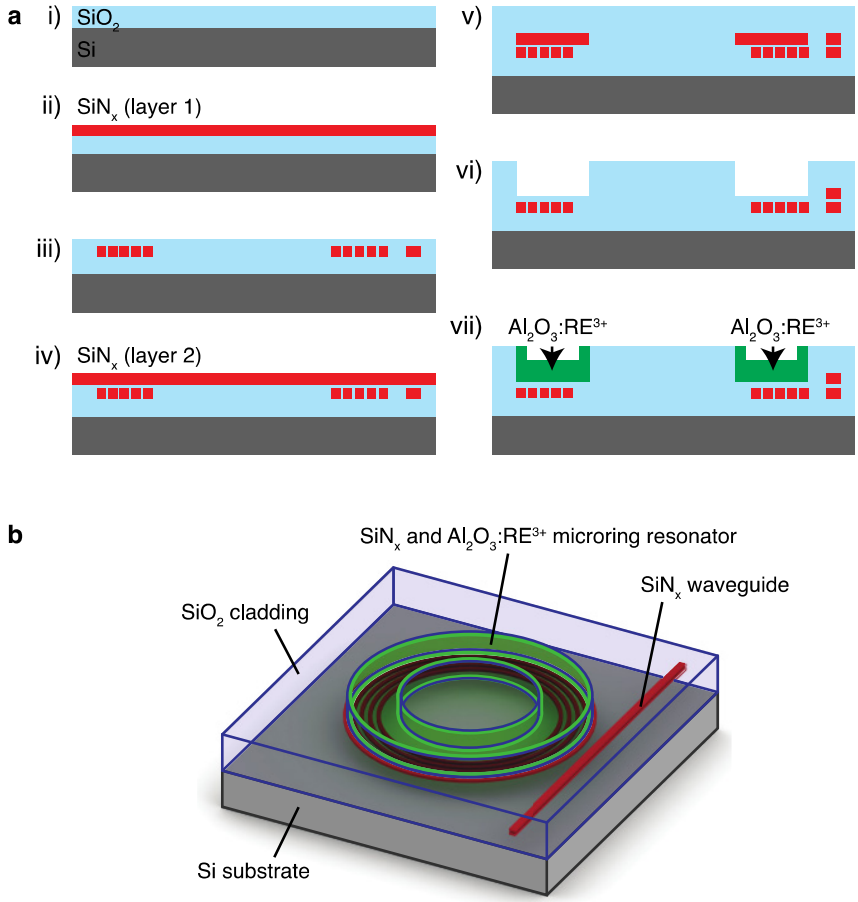

Fig. 1. (a) Silicon-compatible microring laser fabrication steps: (i) deposition of the SiO_2 bottom-cladding layer on a silicon substrate; (ii) deposition of the lower SiN_x layer; (iii) patterning of the SiN_x rings and bottom part of SiN_x bus waveguide (at far right) followed by SiO_2 encapsulation; (iv) deposition of the upper SiN_x layer; (v) patterning and SiO_2 encapsulation of the upper SiN_x layer to define the trench etch stop and top part of the SiN_x bus waveguide; (vi) microring trench etch and removal of SiN_x etch stop; (vii) deposition of the Al_2O_3:RE^{3+} gain medium into the trench. (b) Illustration of the resulting monolithic rare-earth-doped microring laser structure.

We fabricated the microring laser chips using a 300-mm CMOS foundry with a 65-nm technology node. First, we deposited a 6-µm-thick SiO_2 bottom cladding layer on a 300-mm silicon wafer, followed by deposition and patterning of two 240-nm-thick SiN_x (n = 1.94 at 1550 nm) layers with a 100-nm-thick SiO_2 layer in between. We deposited all SiO_2 and SiN_x layers using plasma-enhanced chemical-vapor deposition and surface-polished them after deposition to reduce optical scattering losses. We patterned both SiN_x layers using 193-nm immersion lithography and reactive ion etching, yielding 0.6-µm-wide SiN_x microring features with 0.4-µm separations and 160-µm outer diameter, waveguide widths, w, of 0.4 or 0.9 µm and microring-waveguide gaps, g, ranging from 0.1 to 1.0 µm (in 0.1 µm steps). Above the top SiN_x level, we deposited a 4-µm-thick SiO_2 layer, and patterned and etched 4-

#206846 - $15.00 USD Received 20 Feb 2014; revised 29 Apr 2014; accepted 29 Apr 2014; published 13 May 2014
(C) 2014 OSA

μm-deep microring trenches using the upper SiN_x layer as an etch stop. After removal of the SiN_x etch-stop, we deposited an additional 100-nm-thick SiO_2 layer in the microring trenches. We then etched deep trenches at the edge of the chips for dicing and fiber end-coupling and transferred the wafers from the silicon foundry. Lastly, we diced the wafers into individual dies and deposited 2-μm-thick undoped, erbium-doped and ytterbium-doped aluminum oxide films over the top of the dies (shown only deposited into the microring trenches in Fig. 1 for clarity) using a reactive co-sputtering process similar to that described in [38]. For the ytterbium-doped lasers we applied a uniform doping profile and concentration of 7×10^{20} cm^{-3} We selected a relatively high Yb^{3+} doping concentration because of the low absorption-to-emission cross-section ratio around 1050 nm and negligible concentration-quenching effects observed in Al_2O_3:Yb^{3+} [39]. Moreover, relatively high gain was required to overcome the higher internal resonator scattering losses near 1 μm and output coupling as compared to erbium-doped devices operating near 1.5 μm. For erbium-doped lasers, the erbium concentration was varied throughout the layer in order to match the 980-nm pump mode distribution and minimize the laser threshold. We varied the sputtering power applied to the erbium target throughout the deposition, resulting in uniform lateral doping and a graded vertical concentration profile (with peak in the center of the film and approximately 1/3 the peak concentration at the top and bottom of the film). We selected peak erbium concentrations on the order of $2–3 \times 10^{20}$ cm^{-3} – high enough to achieve higher gain than cavity losses, but low enough to maintain low threshold lasing and avoid significant concentration quenching mechanisms [40]. We summarize the fabrication steps in Fig. 1(a) and the resulting structure is illustrated in Fig. 1(b).

We show images of the fabricated microring lasers in Fig. 2. A top view of the monolithic laser structure is displayed in Fig. 2(a), with the integrated SiN_x bus waveguide visible below the microring. In Fig. 2(b), we show a top-view scanning electron micrograph (SEM) image of the microring trench structure on the silicon chip. Figure 2(c) shows a focus-ion-beam-milled cross-section of the microring-waveguide coupling region at the edge of the trench. The image displays the 2-μm-thick Al_2O_3:RE^{3+} layer on the bottom of the trench as well as a thinner Al_2O_3:RE^{3+} layer deposited on the trench sidewall due to the conformal sputtering process (the material visible above the Al_2O_3:RE^{3+} is metal deposited for imaging purposes). In Fig. 2(d), we display a close-up view of the coupling region, as indicated by the red box in Fig. 2(c). It reveals a slight offset between the top and bottom silicon nitride layers, as well as residual SiN_x etch-stop material at the edge of the trench (both of which fall within the design tolerance of the lasers). Figure 2(d) clearly shows the integrated SiN_x bus waveguide and indicates the waveguide width and microring-waveguide gap.

#206846 - $15.00 USD Received 20 Feb 2014; revised 29 Apr 2014; accepted 29 Apr 2014; published 13 May 2014
(C) 2014 OSA

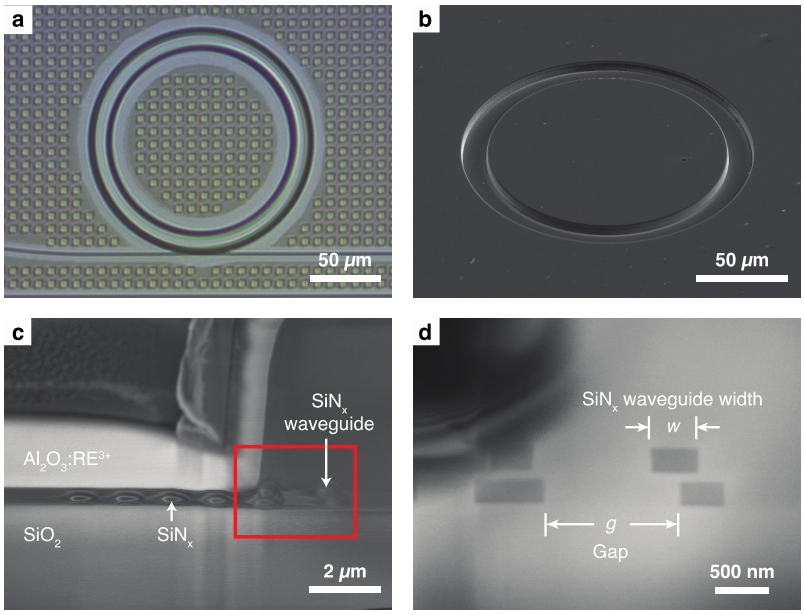

Fig. 2. (a) Top-view optical microscope image of an on-chip rare-earth-doped microlaser showing the integrated microring resonator and SiN_x bus waveguide; (b) scanning electron micrograph (SEM) image of the Al_2O_3:RE^{3+}-filled trench on top of the silicon chip; (c) SEM cross-section image of the edge of the SiN_x and Al_2O_3:RE^{3+} microring resonator; (d) close-up view of the coupling region (indicated by the red box in (c)), showing the SiN_x bus waveguide, waveguide width, *w*, and microring-waveguide gap, *g*.

3. Microcavity and microlaser characterization

3.1 Measurement setup

We carried out transmission and laser measurements using a fiber end-coupling setup. For passive transmission measurements, light from a fiber-coupled 960–990-nm tunable laser (< 200 kHz linewidth, 1-pm minimum step size) or 1460–1630-nm tunable laser source (100-kHz linewidth, 0.1-pm minimum step size) was coupled through a polarization controller and end-coupled to the chip via a single-mode 980-nm (SM980) cleaved fiber. We coupled light from the chip using another SM980 cleaved fiber and measured the transmitted optical power using an InGaAs detector. For laser measurements, on the input side, pump light from the 960–990 nm tunable laser source or a 976-nm diode laser (1-nm linewidth) was coupled to a polarization controller, followed by a 980-nm variable-optical attenuator (VOA), a 99%/1% tap and a 980/1050 nm (Yb-doped microring lasers) or 980/1550 nm (Er-doped microring lasers) fiber-based wavelength division multiplexer (WDM). We coupled light to and from the chip using SM980 bare fibers and coupled the output fiber to another fiber WDM to separate the residual pump and laser light. We adjusted and monitored the incident pump power using the VOA and output from the 1% branch of the tap, respectively. We measured the laser output powers and optical intensity spectra by coupling the 1050 or 1550 nm branch of the WDM from each side of the chip to an optical spectrum analyzer (600–1700 nm, 20-pm resolution). Time domain measurements were carried out by coupling the laser output to an amplified 10-MHz photodetector connected to an oscilloscope.

3.2 Passive transmission measurements

Figures 3–5 summarize 980-nm and 1550-nm transmission measurements in undoped (passive) microrings. In Fig. 3, we show the resonantly-coupled 980-nm pump power vs.

#206846 - $15.00 USD Received 20 Feb 2014; revised 29 Apr 2014; accepted 29 Apr 2014; published 13 May 2014
(C) 2014 OSA

microring-waveguide gap. We measured the coupling for the transverse-electric- (TE-) and transverse-magnetic- (TM-) like pump modes near 980 nm (labeled TE1 and TM1, see Fig. 4) and w = 0.4 µm (the same waveguide width as for Er- and Yb-doped microring lasers). For both polarizations we observed optimum coupling near g = 0.5 µm, where the internal quality factor of the resonator, Q_i, matched the external quality factor, Q_e [41].

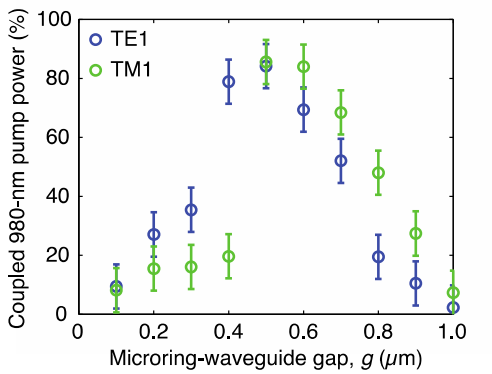

Fig. 3. 980-nm pump coupling in undoped microrings with w = 0.4 µm and microring-waveguide gaps ranging from 0.1 to 1.0 µm. Maximum coupling for both TE and TM polarizations occurs at gaps near 0.5 µm, where the internal and external quality factors of the resonator are matched.

Figure 4 (top) shows 980-nm transmission measurements for a device with w = 0.4 µm and g = 0.7 µm and both TE and TM polarizations (left and right, respectively). The insets show the intensity profiles of the optimum pump modes (TE1 and TM1) calculated using a finite element mode solver, with their resonances indicated on the plots. Their resonances were differentiated from those of the lowest order TE and TM modes (TE0 and TM0), which calculations show are strongly confined in the SiN_x layer, and higher-order, lossier modes by their free-spectral ranges, 1.10 and 1.12 nm, respectively. By fitting the high-resolution transmission responses of the under-coupled resonator using a Lorentzian function (Fig. 4, bottom) [41], we obtain internal quality factors, Q_i, of 3.8×10^5 and 2.7×10^5 (TE1 and TM1, respectively). These Q_i correspond to propagation losses per unit length of 1.3 and 1.8 dB/cm at the pump wavelength in the cavity.

Figure 5 (top) shows 1550-nm transmission measurements in similar ring structures with w = 0.9 µm (phase matched to the 1550-nm resonator modes) and g = 1.0 µm. The inset images show the calculated intensity profiles of the TE1 and TM1 modes. By fitting the resonances (Fig. 5, bottom), we obtain Q_i on the order of 5.7×10^5 and 4.2×10^5 for TE and TM polarization, respectively. These quality factors correspond to propagation losses of 0.5 and 0.7 dB/cm. Given the peak gain coefficients of 2.0 dB/cm at 1532 nm and 2.5 dB/cm at 1020 nm measured previously in Er- and Yb-doped Al_2O_3 waveguides [39,40], we determined such passive resonator losses to be sufficiently low so as to enable round-trip net gain and lasing in the rare-earth-doped microrings.

#206846 - $15.00 USD Received 20 Feb 2014; revised 29 Apr 2014; accepted 29 Apr 2014; published 13 May 2014
(C) 2014 OSA

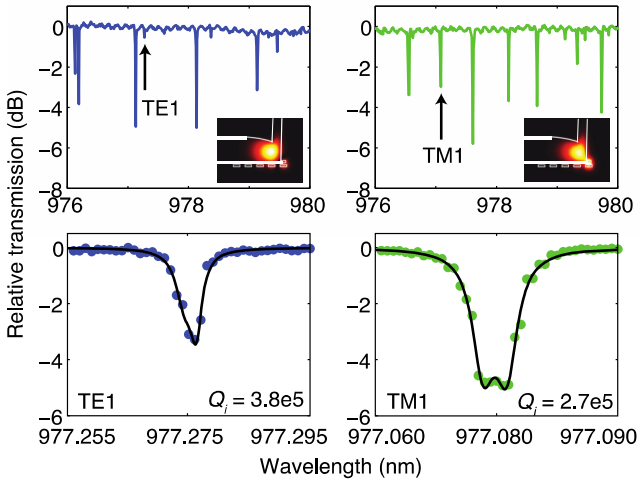

Fig. 4. 980-nm transmission measurements in an undoped microring with w = 0.4 μm and g = 0.7 μm. The top plots were measured over a scan range of 4 nm (10 pm step size) and show coupling to multiple TE-like (left) and TM-like (right) resonances. The optimal calculated Er- and Yb-doped microring pump modes (TE1 and TM1) are shown in the insets and their resonances indicated on the plots. Bottom: high resolution (1 pm step size) scans of single TE1 (left) and TM1 (right) resonances. By fitting the data using a Lorentzian function we determined internal quality factors, Q_i, of 3.8×10^5 and 2.7×10^5.

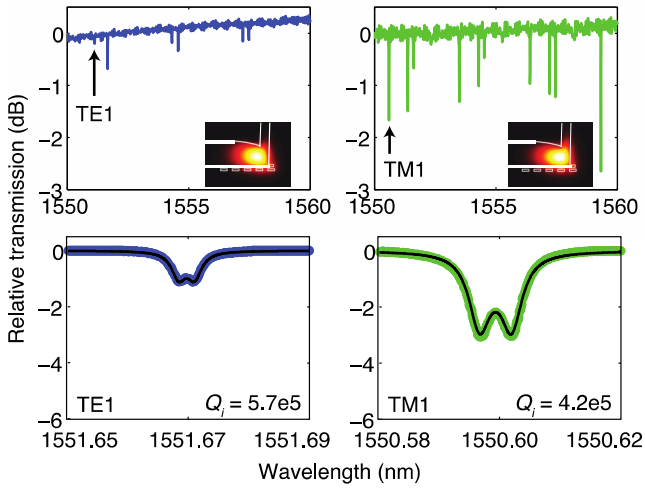

Fig. 5. 1550-nm transmission measurements in an undoped microring with w = 0.9 μm and g = 1.0 μm. The top plots were measured over a scan range of 4 nm (1 pm step size) and show coupling to multiple TE-like (left) and TM-like (right) modes. The calculated optimum 1550-nm Er-doped microring laser modes (TE1 and TM1) are shown in the insets and their corresponding resonances in the undoped microrings indicated on the plots. Bottom: high resolution (0.1 pm step size) scans of single TE1 (left) and TM1 (right) resonances. By fitting the data using a Lorentzian function we determined internal quality factors, Q_i, of 5.7×10^5 and 4.2×10^5 for the 1550 nm TE-like and TM-like modes, respectively.

3.3 Microring laser measurements

We observed laser emission in both Er- and Yb-doped microrings. In Fig. 6 we show an optical microscope image of a resonantly-pumped Er-doped microring laser. The image displays the typical green spontaneous emission from excited Er^{3+} ions due to excited state

#206846 - $15.00 USD Received 20 Feb 2014; revised 29 Apr 2014; accepted 29 Apr 2014; published 13 May 2014
(C) 2014 OSA

absorption and ion-ion interactions. At different gaps we observed laser modes spanning a wavelength range of 1530–1565 nm and both multi-mode and single-mode lasing. The laser spectrum was typically multi-mode at low pump powers (i.e. the maximum power obtainable with the tunable laser), while one or two dominant modes emerged under higher powers (typically requiring 976-nm diode laser pumping). As shown in Fig. 7, for a device with peak Er concentration, $N_{Er,peak}$, of 3×10^{20} cm^{-3} and $g = 0.3$ µm we observed single-mode lasing at 1559.82 nm (with side-mode suppression > 30 dB) and up to 27-µW total laser power in the silicon nitride waveguide (limited by the maximum diode laser pump power). By comparing to the resonances observed in 1550-nm transmission measurements in the same chips, we determined the laser modes to be TM-like. The free-space −3dB linewidth was < 20 pm (below the limit of the optical spectrum analyzer used to measure the laser spectrum). We obtained the lowest laser threshold in devices with g ≈0.5 µm (at optimum pump coupling) and at reduced erbium concentration. In Fig. 8, we show the laser power curve of a device with $N_{Er,peak} = 2 \times 10^{20}$ cm^{-3} and $g = 0.5$ µm measured under resonant pumping at 978.84 nm, near the Er absorption peak. The laser exhibits a threshold of 0.5 mW, and double-sided slope efficiency of 0.3%, with up to 2.4 µW output power (total power measured from both outputs) coupled into the SiN_x waveguide. Time-domain measurements in several devices revealed that the lasers operated in a pulsed mode at frequencies on the order of 1 MHz, as observed in previous erbium-doped lasers [42–44].

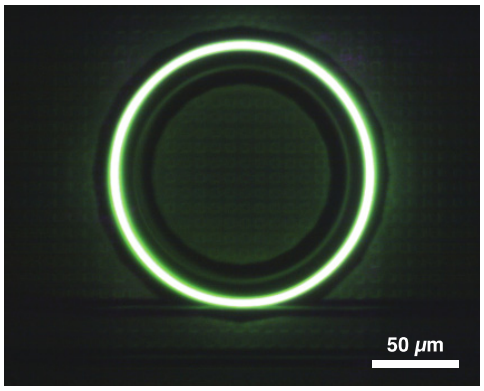

Fig. 6. Top-view of an Er-doped microring laser injected with 980-nm pump light, showing the characteristic spontaneous green-light emission from excited Er^{3+} ions.

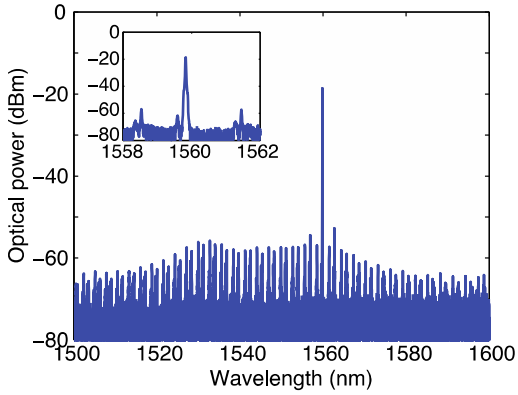

Fig. 7. Emission spectrum of an Er-doped microring laser with $N_{Er,peak} = 3 \times 10^{20}$ cm^{-3} and $g = 0.3$ µm and pumped using a laser diode centered at 976 nm. The output is single-mode at 1559.82 nm with a side-mode suppression of > 30 dB.

#206846 - $15.00 USD Received 20 Feb 2014; revised 29 Apr 2014; accepted 29 Apr 2014; published 13 May 2014
(C) 2014 OSA

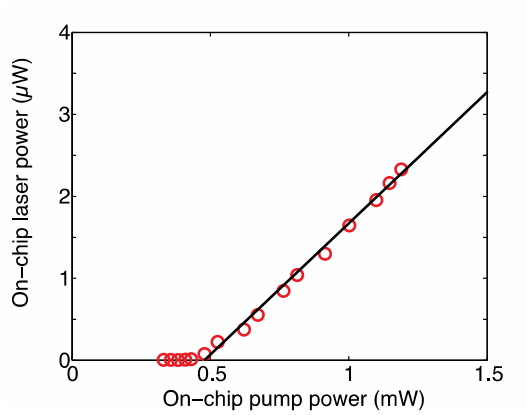

Fig. 8. Output power vs. on-chip 978.84-nm pump power for an Er-doped microring laser with $N_{Er,peak} = 2 \times 10^{20}$ cm^{-3} and $g = 0.5$ μm. The laser threshold is 0.5 mW and the double-sided slope efficiency is 0.3%.

In Yb-doped microrings we observed lasing on multiple TE- and TM-like modes and at wavelengths in the range 1020–1045 nm. In Figs. 9 and 10, we show typical Yb-doped microring laser measurements, obtained for $g = 0.4$ μm. We observed lowest-threshold lasing at a pump wavelength of 970.96 nm when tuned onto the TM-like resonance. This wavelength is blue-shifted from the Yb^{3+} absorption peak around 975 nm because the absorption at 975 nm is too strong, thus significantly reducing both Q_i and the coupled pump power. The laser spectrum under maximum pump power is displayed in Fig. 9. A single laser line is evident at 1042.74 nm with a side-mode suppression of > 40 dB (inset). The laser power curve for the same microring laser is shown in Fig. 10. We observed lasing at a threshold of 0.7 mW, a total output power of > 100 μW coupled into the SiN_x waveguide and double-sided slope efficiency of 8.4%. As with the erbium-doped microring lasers, we observed pulsing behavior at pump powers close to threshold, with pulse frequencies up to 2 MHz. With increasing pump power, however, the pulsing behavior was eventually suppressed and we observed continuous-wave, single-mode lasing in Yb-doped microrings.

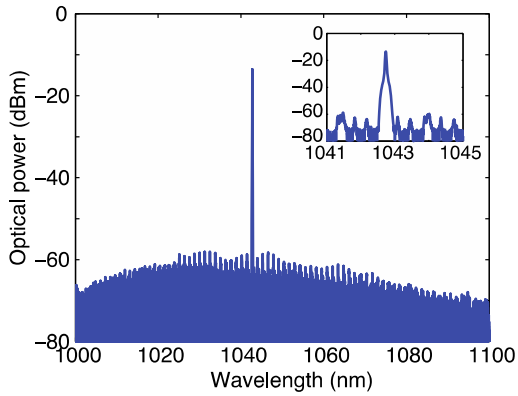

Fig. 9. Emission spectrum of an Yb-doped microring laser with $g = 0.4$ μm and under resonant pumping at 970.96 nm. The output is single-mode at 1042.74 nm with a side-mode suppression of > 40 dB (inset).

#206846 - $15.00 USD Received 20 Feb 2014; revised 29 Apr 2014; accepted 29 Apr 2014; published 13 May 2014
(C) 2014 OSA

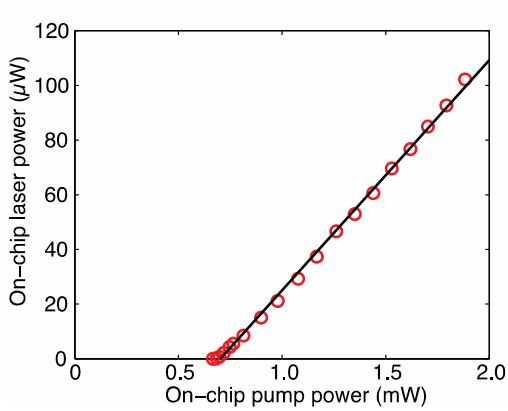

Fig. 10. Output power vs. on-chip 970.96-nm pump power for an Yb-doped microring laser with g = 0.4 µm. The laser emits > 100 µW power into the integrated SiN_x waveguide, with a lasing threshold of 0.7 mW and double-sided slope efficiency of 8.4%.

4. Discussion

With these results we have realized highly-compact monolithic rare-earth-doped devices on silicon. Previously, the smallest bend radius obtained in an $Al_2O_3:Er^{3+}$ device embedded in SiO_2 was 250 µm, in that case a compact amplifier [45]. Here, using SiN_x features we reduce the bend radius to 80 µm, thus suggesting a path towards more compact integrated amplifiers as well as lasers. Compared to previous $Al_2O_3:Er^{3+}$ racetrack lasers [16], we have decreased the device footprint by a factor of ~500. In addition, we show single-mode operation, which is much more easily obtained in a smaller resonator structure. Meanwhile, the total cavity length of the microrings is 20 times shorter than that of DFB and DBR devices [17–21], and the thresholds reported here are more than 10 times smaller.

While in this work we demonstrate a proof of principle, a full investigation of the parameter space can lead to enhanced microring laser performance. Continuous-wave operation of erbium-doped microlasers can be achieved by injecting higher pump powers (as demonstrated in the ytterbium-doped microring lasers and [21]) or by adjusting the $Al_2O_3:Er^{3+}$ layer thickness and doping concentration [42]. In addition, Er-Yb co-doping or in-band pumping at 1480 nm can be explored to increase the erbium laser efficiency. Furthermore, the high efficiencies of DFB and DBR REDWLs [17,18] and ultra-low thresholds demonstrated in fiber-coupled microcavities [24–31] indicate that higher efficiencies and lower thresholds can be obtained by optimizing the resonator mode and optical coupling properties and increasing the cavity Q.

By using standard silicon wafer-scale processing, we demonstrate that these microring lasers can be implemented in silicon-based photonic circuits (*i.e.* enabling integration with high-performance active and passive silicon, germanium and silicon nitride devices). A single off-chip fiber-coupled pump source or heterogeneously-bonded on-chip laser diode pump could efficiently power multiple microring lasers. Due to their low threshold and single-mode operation around 1.5 µm, arrays of Er-doped lasers are promising as chip-scale multi-wavelengths communications sources. Meanwhile, Yb-doped lasers emit in the low water absorption window, can operate in water and can act as highly effective nanoparticle sensors [46,47]. Thus, their implementation in lab-on-a-chip or integrated biophotonic applications is of interest. Furthermore, the reported cavity structure can easily be adapted for additional rare earth dopants (Nd^{3+}, Tm^{3+}, etc.) with different pump and laser wavelengths.

5. Conclusion

In summary, we have shown lasing in fully-integrated, monolithic microring structures on silicon chips. The rare-earth-doped microring lasers are enabled by a multilayer design which

#206846 - $15.00 USD Received 20 Feb 2014; revised 29 Apr 2014; accepted 29 Apr 2014; published 13 May 2014
(C) 2014 OSA

is silicon-compatible, straightforward and can be easily adapted to realize laser sources emitting from the visible to mid-infrared wavelengths on a full silicon photonics process flow. The low lasing threshold observed in both erbium- and ytterbium-doped lasers suggest that a single, low-cost diode laser pump source could excite densely-integrated arrays of lasers on a chip for wavelength division multiplexing applications. Optimization of optical coupling parameters and microring mode properties can lead to even lower thresholds, higher efficiencies and smaller device footprints. These new, compact, inexpensive and efficient lasers are a viable alternative to existing silicon-based laser technologies and have implications for wide-ranging applications of integrated photonic systems, including optical computing, classical and quantum communications, sensing, biophotonics and fundamental micro- and nanoscale research.

Acknowledgment

This work was supported by the Defense Advanced Research Projects Agency (DARPA) of the United States under the E-PHI project, grant no. HR0011-12-2-0007. Fabrication was carried out in part at the College of Nanoscale Science and Engineering at the State University of New York and the Microsystems Technology Laboratories at the Massachusetts Institute of Technology. We thank K. Broderick and T. Yu for their assistance with fabrication and imaging.